https://doi.org/10.3311/PPci.20867

Periodica Polytechnica Civil Engineering, 67(1), pp. 177–188, 2023

In-situ Primary Stress Detection Based on Seismic Tomography Measurements and Numerical Back-analysis for an Underground Radwaste Repository

Ferenc Deák[1,3,4*], Matthew A. Perras[2], János Bakai[3], Ákos Török[1]

[1] Department of Engineering Geology and Geotechnics, Faculty of Civil Engineering, Budapest University of Technology and Economics, Műegyetem rkp. 1, H-1111 Budapest, Hungary
[2] Department of Civil Engineering, Lassonde School of Engineering, York University, 204 Bergeron Centre, ON M3J 2S5, Toronto, Canada
[3] Geopolita Ltd., Platánfa utca 59, H- 2030 Érd, Hungary
[4] SeklerGeo, Újfasor, 28, H-7630 Pécs, Hungary
[*] Corresponding author, e-mail: deak.ferenc@tunnelte.ch

Received: 23 July 2022, Accepted: 30 October 2022, Published online: 17 November 2022

Abstract

In order to understand how the in-situ primary stress state has evolved with subsidence and uplift in a granitic rock mass for anticipated of a radioactive waste repository in Hungary, the authors investigated the applicability of seismic tomography as an interpretive tool. Very high P wave velocity (V_p) values were obtained during the tomographic scanning of the study area of the repository, and these were compared with existing findings of in-situ and laboratory seismic measurements.

Apart from seismic tomographic survey, dynamic FEM numerical modelling, empirical calculations of residual stresses, laboratory measurements of compression wave (ultrasonic) velocities on intact rock cores, in-situ primary stress measurements as well as site geological model were integrated to evaluate the use of seismic tomography for identifying possible in-situ stress increases around the excavation.

A detailed calibration modelling was carried out based on the site seismic tomography measurements and during the large-scale modelling. It was observed that the increasing V_p is directly related to simulated increasing directional loadings on the rock mass. Using a measured wave raypath it was possible to check the different in-situ stress parametrizations which resulted in the best approximation to the measured V_p values.

It was concluded that the rock mass under investigation to extend the repository must have higher in-situ stress values than the area of the constructed deposition chambers nearby. The results of this research indicated that seismic tomography is a useful tool for determining relative stress around and within the vicinity of underground excavation.

Keywords

in-situ stress, seismic tomography, dynamic modelling, wave velocity, raypath

1 Introduction

Deep geological repositories (DGR) for the storage of radioactive waste are typically designed for sealing radionuclides from the surrounding environment for up to one million years. The engineered barriers that are placed around the waste, in combination with the natural barrier provided by the rock mass, contain the radioactive waste and isolate the radionuclide contaminants from migrating into the surround area for the long design lifetime.

The National Radioactive Waste Repository (NRWR) for low and intermediate level waste (LLW/ILW) in the Bátaapáti area, has been located in a granitoid formation, which will be used for the final disposal of LLW/ILW from domestic nuclear power plants in Hungary. This repository is not a typical DGR, which are typically located at depths of approximately 500 m or more, but rather with an overburden thickness or depth below ground of 240–270 m. Based on the authorization contained in the Hungarian Atomic Act, the tasks related to the construction and operation of the NRWR are conducted by the Public Limited Company for Radioactive Waste Management (PURAM) of Hungary.

Characterizing and examining the evolution of the stress state, including stress increases in different rock

Cite this article as: Deák, F., Perras, M. A., Bakai, J., Török, Á. "In-situ Primary Stress Detection Based on Seismic Tomography Measurements and Numerical Back-analysis for an Underground Radwaste Repository", Periodica Polytechnica Civil Engineering, 67(1), pp. 177–188, 2023. https://doi.org/10.3311/PPci.20867

mass blocks, stress concentrations and stress relaxation, is of importance when trying to mitigate geohazards or to characterize the possible in-situ stress state around the potential repository.

Zang and Stephansson [1] published that certain measurement methods, which allow for accurate measurement of stress magnitudes, only represent a very small area of the rock mass surrounding the measurement point. For instance, the rock mass volume involved in overcoring measurements (doorstopper and CSIRO cells were used in the NRWR) is small with the possible dimension of the stress field analyzed being between 10^{-3} to 10^{-2} m^3. Other measurement methods, such as hydraulic fracturing, account for a large volume of the rock mass between 0.5 to 50 m^3.

Several authors [2, 3] have shown that stress fields are correlated with stress indicators, such as seismic velocity. Previous studies have shown a significant non-linear increase in seismic velocities with a small rise in the hydrostatic pressure [2, 3].

The rock mass responds to variations in the stress state of the underground cavities. For example, high-stress areas typically have closed microcracks in the rock mass and hence have an increase in seismic velocities. By mapping the velocity variations as a function of space and time, one can begin to understand the stress variations associated with extraction of the rock mass during construction of new underground area. Tomographic imaging of mines have been used to determine the stress distribution around mines in several studies (e.g., [4–7]). Some studies have shown excellent results when using these techniques to monitor the stability of block caving operations [8, 9]. Previous seismic tomographic studies (e. g., [10–16]) have shown that seismic tomography can be used to determine relative stress.

The increase in velocity can be related to the closure of void space, for instance pores and cracks. In general, the degree of velocity increase is nonlinear and greatest with an early incremental increase in stress. As the stress increases during excavation, the degree by which the velocity increase is reduced in response to the formation of new cracks (yield point) parallel to the loading direction. The work cited above all suggest that regions of high velocity are likely an indication of zones of high stress concentration, whereas low velocity regions indicate zones of stress relaxation and damage.

In this study, is demonstrating that the distribution of P-wave velocities, both a temporally and spatially, can support the interpretation of stress variations and ultimately help better characterizing the stress state around an underground opening.

2 Geological setting of the Bátaapáti Repository Site

The Bátaapáti NRWR repository site area is located in the north-eastern part of the Mórágy crystalline block, which is the northernmost part of the Tisza unit and belongs to the Mecsek zone. Geographically it is located near the village of Bátaapáti (Fig. 1).

The pre-Cenozoic formations of the Mórágy Block predominantly granitoid rocks classified as the Mórágy Granite Formation. The granite body is oriented in an NE – SW strike and is bounded from the northwest by the tectonic Mecsekalja Belt, which also has an approximately NE – SW strike and a steep NE-NW dip. In this belt the Paleozoic metamorphic formations of the Ófalu Formation Group [17–19] are located. The main characteristics of the granitic block that hosts the site are discussed below and are based on the underground investigations conducted by PURAM.

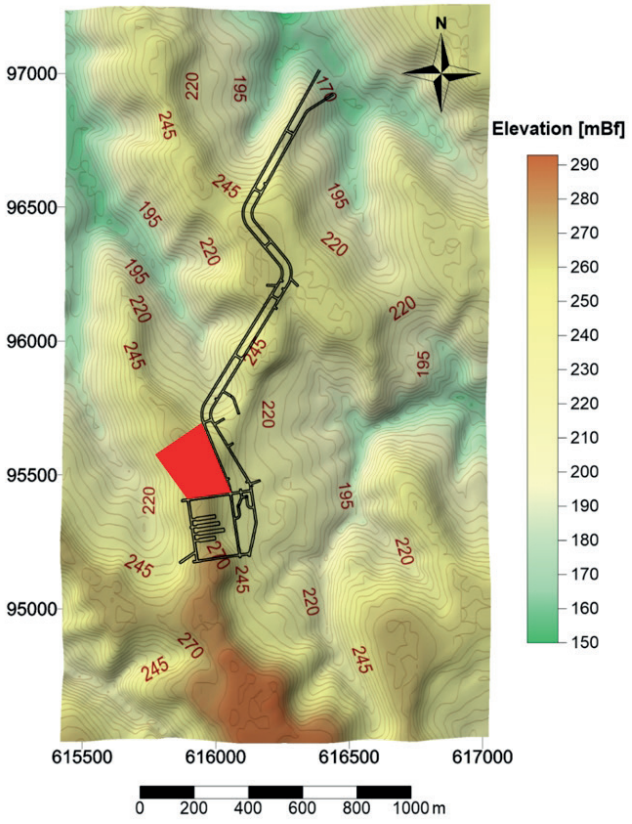

Fig. 1 Elevation map (meters above the Baltic Sea, mBf) of the excavated radwaste repository underground facilities, with red indicating the investigated seismic tomography area and black representing the excavated tunnels of the Bátaapati site

At the repository chambers level, at an absolute height of ±0 mBf (above the Baltic Sea level), the most important geological structure of the eastern part of the chamber area is the banded-striped structure. The strike of the bandings is NE-SW. Three main petrological bands can be distinguished in the area, which are as follows from north to south:

Northern monzonite band: the northern area is excavated for the Storage Conveyor Trench or access tunnel. This twin tunnel lies predominantly in the monzonitic layer south of the 6th cross passage tunnel, intersected by a 0.6–1.9 m thick alkaline volcanic vein with a steep dip to the NE–SW. The vein is accompanied, in the same orientation, by a fracture zone varying in the quantity of the clay mineralization. The fracture zone with open cracks can reach a transmissivity of 10^{-5} m^2/s.

Middle, monzogranite band: The northern boundary of the middle band, containing rarely porphyry monzogranite. It continues towards the storage chambers along the fractured, aquifer zone accompanying the alkali basalt vein. It has a predominantly monzogranite composition and develops from the north with a gradual transition from monzonites (with contaminated monzonite and contaminated monzogranite hybrid rock variants). Its southern boundary is essentially the "Patrik Fracture" fault zone (officially known as "17-NE-SW") and the accompanying fragmented rock zone.

Southern, mixed rock band: The southern band is bounded on the north by the "Patrik Fracture". This 10–15 m thick fracture zone is a structure of primary importance with a variable internal structure of one or more clay core zones. Its strike is predominantly NE-SW, its plunge is steep in the SE direction. The rocks that make up the band change from a monzogranite composition to the altered monzogranite and contaminated monzonitic composition in a SE direction. The predominant rock material of the southern mixed rock band is contaminated monzogranite, which contains island-like contaminated monzonite and monzonite lenses with a horizontal extent of 10–15 m and an elongation to the NE-SW.

3 Geotechnical background

Based on the experience during the construction of the existing tunnels, the rock mass quality in the Mórágy Granite – and thus the expected geotechnical conditions – are determined by fractures and fracture networks formed as a result of past tectonic activity of the area. Former investigations identify [17, 18] six main paleo-stress fields, including an extremely large number of fracture networks in different directions and generations, based on core scanner imaging. The various fracture systems were deformed in different ways and to different extents due to the varying stress fields, reopened and further developed. As a result, a dense network of fracture zones and cracks with extremely variable sizes, orientations and infilling materials have evolved. The spatial course of individual fractures is usually irregular and difficult to track due to other tectonic phenomena. The exact location of their occurrence is most often unpredictable. As a result of the research, it was also found that in the case of filling fractures that can be classified into phases separated on the basis of individual stress field directions, it is not possible to identify typical fracture-infilling materials [20]. In addition to the individual fractures at the site, the thicker fracture belts, in the order of up to 10 meters, are of important significance from both a geotechnical and hydrogeological point of view, most of which are characterized by clay mineral infilling.

Due to the geological and tectonic prehistory of the Mórágy Granite Formation, the rock mechanical-geotechnical parameters show extreme inhomogeneity, and thus their spatial extensibility at the site and its surrounding is rather limited.

The inclined access tunnels and the repository chambers, in many cases cross large-scale alkali vulcanite veins. Mostly, these are reported to indicate a marked change in the documentable quality of the rock mass. The high degree of rock quality deterioration was caused by the fragmented, crumbled, brecciated zone of this damage zone in the case of the seed zones. While in the case of the veins the brittle fractures and the intensity of water seepage also increased.

In the case where excavations crossed larger fault zones (such as the Klára or Péter fault zones), the core zone and its boundary consisted of decomposed clay, soil-like material, which should be characterized by a soil mechanics approach during the design. For these zones, the Mohr-Coulomb failure criterion (and constitutive model) should be used instead of the Hoek-Brown failure criterion, which can be used elsewhere.

4 The seismic refraction survey

Measurement of the seismic wave velocity propagating in intact laboratory rock samples and in rock mass has been used for decades to map rock types, rock quality, stress-strain change, and to determine physical and dynamic rock characteristics. In general, the arrival of the primary (P) or longitudinal wave is measured as the first arrival and the secondary (S) or the transverse wave, can only be detected with the appropriate sensors and arrives the second.

In-situ measurements can be conducted using, for example a probe that has perpendicular sensors with extremely high directional sensitivity and the excitation detection is close to the line of the probe's body. Another sensor configuration is to measure the two wave types however, the sensors must be separated a sufficient distance to be able to distinguish the arrival of the S wave clearly.

In the series of measurements performed in this study, the primary goal was to determine the velocity of the P-wave, and only in some cases were the S wave velocities determined.

First, the measurements were performed in two near horizontal boreholes (in BeR-19 and BeR-20) enclosing the examined area. With this arrangement, a more detailed picture of the P-wave velocity field was obtained, compared to when a rock pillar was instrumented in a survey with only sensors (receivers) placed on the surface of the investigated cavity wall. Both on the excitation (by sources) and on the receiver side, there was expected to be a decrease in V_p due to the excavation damaged zone (EDZ). With the borehole measurements used in this case however, the incoming signal (first arrival) at the sensor placed in the boreholes is not distorted due to EDZ, as the boreholes extend past the EDZ.

The frame of reference used considered the borehole mouth as a distance of 0 m and the other end of the borehole as 10 m from the start of the borehole. To have a better resolution tomogram, receiver sensor points were placed on the access tunnels walls, as shown in Fig. 2.

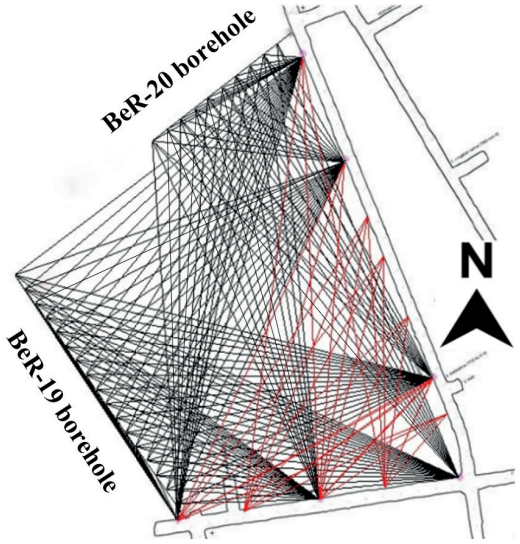

Fig. 2 The planned raypaths (black lines) with receivers in the boreholes and the additional raypaths (red lines) with receivers on the tunnel walls

Fig. 3 Seismic wave propagation using a hammer at the source point on the tunnel wall

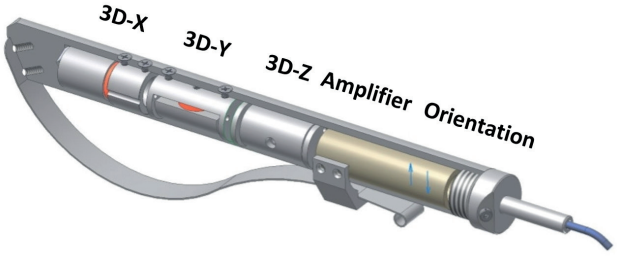

Fig. 4 Schematic drawing of the measuring probe

4.1 Deployed instruments

During the measurements, the source points were marked on the shotcrete wall and in several cases, for instance at corner points we drilled little anchors to make direct contact with the rock mass through the shotcrete. The signal excitation was performed with a hammer blow of 5 kg within the circle marked with the paint spray (Fig. 3).

The measurements were performed with a high-sensitivity probe used in both BeR-19 and BeR-20 boreholes. Following the borehole measurements, the probe was fixed to the shotcrete walls using a specially manufactured clamping device, which was mounted on a drilled 8 mm diameter screw. The accelerometers giving the trigger signal were fitted to the drilled bolts on the shotcrete layer, near to the source, their distance was measured with a tape. The measuring probe has been specially designed for the measurements conducted in this study (Fig. 4).

The probe contains three piezoelectric sensors perpendicular to each other with high sensitivity. In the Z direction, a sensor with the same directional sensitivity as the axis of the measuring probe was installed, and the X and Y sensors are perpendicular to the probe axis. The outputs of the built-in X and Y direction sensors were connected for greater sensitivity. Therefore, the built-in direction finder sensor was not used in this case, as the X and Y directions could not be separated from the signal thereby the signals

were summed. The built-in piezo sensors had an extreme sensitivity of 0.025 mV/(m/s^2). The probe was powered by an independent power source located in the box beside the datalogger, and the signals were also routed through a 5-wire shielded cable that provided complete noise protection.

4.1.1 Computing background – hardware and software

A Dell 520D computer received signals from an Advantech USB 4711A A/D converter and recorded them at the same time for all the measurements. The A/D converter used in the measurements could sample at a speed of 150000 samples/s, so each channel was recorded at a density of 50000 samples/s. The A/D converter that was used had a resolution of 12 bits and a range of ±0.625 V, which means an additional four times the amplification, so the smallest detectable signal was 3×10^{-6} m/s^2.

The program running on the computer (a self-developed VBA code) continuously stored the signals from the moment of starting the program, while also displaying it on the screen. This allowed to check in real time whether signals were being received, the reference sensors were working, and the quality of the current recording.

It was possible to review individual recordings on site, even immediately. This program system guaranteed that the maximum information was extracted from the measurements.

4.2 Evaluation of measurement data

A separate binary data file was created for each pair of measurement points (source and receiver). The duration of the total wave propagation was recorded in the file, so it was possible to select later triggers and select the appropriate first arrivals.

A separate program was prepared for reading the logged files, which included the individual receiver and source coordinates. Individual recordings could be downloaded and displayed. Based on the first arrivals and where the length of the raypaths allowed for it, S waves could also be identified separately. The velocity values were written down after selection and approval, then saved to a separate file.

As a result of the summed signals (from minute 5 hammer hits), the stochastic noises were eliminated and the signals from the source were amplified. With this procedure, the velocity of the P-wave was determined for all points. As expected, due to the wave propagation in the absorption medium, the high-frequency signals shifted to lower frequencies, but were still suitable for readings with an accuracy of 0.1 ms.

The area was further examined using inversion procedures by Reflexw software with the SIRT (Simultaneous Iterative Reconstruction Technique) algorithm.

In the tomographic processing of the seismic survey measurement data, the "scanned" velocity field could be reconstructed from the measurement geometry and the arrival time data. One of the most successful procedures for this purpose was SIRT. The application requires the recording of the exact geometric data of the source-receiver pairs and the boundary conditions (starting velocity field). The arrival time of a wave can be given as the sum of the time spent in each cell of a range divided into cells [21]. The inversion algorithm modifies the model field in the direction of the better match based on the differences in the runtime values calculated by the model parameter of the cells in each iteration step and the measured. If the difference between the measured and calculated arrival times is less than the measurement error, the calculated velocity field is considered to be the same as the actual velocity field.

Curved radius tomography, which is closer to reality, requires more iteration steps because the radii also changes as the velocity field is modified. Reflexw software uses a finite difference approach to calculate curved radii. The first step is to define the initial model. The initial model may be a simple constant velocity without prior notice, but may consist of a complex layered model, such as that resulting from a previous wavefront inversion. The resulting velocity model is stored in a raster file in the Reflex format, which provides all the possibilities for further interpretation and processing.

During the inversion procedure 15 iterations were set, however, already in the 6th iteration good results were obtained and the inversion ran stably. The matrix of the generated confidence file (as well as the grid files created later from it) allowed for the generation of maps with other scientific content based on different P-wave velocities during subsequent correlation calculations. This file also contained the raypaths counted by tomography. The finalized and smoothed tomogram in Surfer program is shown in Fig. 5.

5 Rock mechanical aspects

Using different geophysical methods, the rock mechanical properties of the rock mass or intact rock samples can be examined without destruction. This is also the case for seismic measurements. In addition to the material properties and cracked nature of the rock, the wave propagation velocities are also affected by the existing stress field during the measurement.

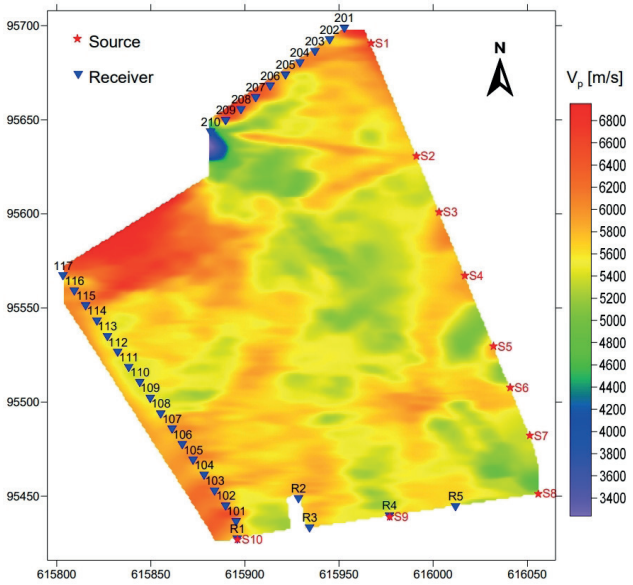

Fig. 5 The finalized and smoothed V_p tomogram

Compared to the previous in-situ seismic tomographic measurements carried out to the South of the current tomogram, near to the excavated repository chambers, they showed much lower V_p values.

It is not recommended to compare or directly extend the database generated during laboratory measurements to the rock mass, because intact rock samples lack representative fractures that are present in the rock mass. In addition, measurements conducted in the laboratory are performed using ultrasonic wave propagation, which is different from the frequency range of seismic waves [22] used in in-situ measurements.

From the laboratory database, with measurements on 550 samples, the following results are characteristic: minimum V_p = 3.65 km/s; maximum V_p = 6.92 km/s.

6 Numerical modelling

In Bátaapáti NRWR, the design of the entire underground facility was made on the basis of static numerical modelling. Knowledge of the dynamic behavior of the rock mass is of great importance, as in many cases dynamic loading can result in a degrading load on the underground structures. For example, blasting in the close vicinity of the cavities can generate 200–300 g accelerations at high frequency in the range of 1–2 s, while earthquakes also act with different energies, at a low frequency but on a time scale of several tens of seconds. In some cases, such as the EDZ or water sealing zones, the dynamic factor can also have a positive effect such as closing fractures.

Deák et al. [23–25] achieved good results in the dynamic examination of larger areas in the case of the Bátaapáti NRWR, where the authors used the dynamic effects of the blasts and earthquakes. Due to the calibration, the damping values, boundary conditions and input parameters of the given area were adjusted so that the resulting seismograms were in good correlation with the time series produced by the measurements.

This seismic tomographic research provided an additional opportunity to refine the aforementioned studies and to extend them to a larger underground area. In this article the continued investigation and further dynamic numerical modeling, which focuses on impact on the EDZ and the dynamic characterization of the rock mass are presented. For numerical modelling, the RS^2 finite element software was used, whose dynamic engine allows to perform the tasks outlined above.

During the dynamic calibration modelling for present study was used a time history chosen from the measured hammer hits at the source points (Fig. 6)

6.1 Model geometry

RS^2 is a 2D FEM software, hence it is necessary to simplify the 3D space encapsulating the measurement space, was created a planar geometry based on the X and Y directions by using EOV (Hungarian Uniform National Projection system). Followed by defining rock types and major fractures marked on the basis of geological mapping in the geometry. The models were produced with the axisymmetric setting.

For the rock mechanical parameterization, published input values from the Geotechnical Interpretation Report [26] were used for material model the generalized Hoek-Brown criterion [27, 28] and in case of constitutive models Hoek-Brown criterion and DISL (Damage Initiation and Spalling Limit) were chosen [29, 30].

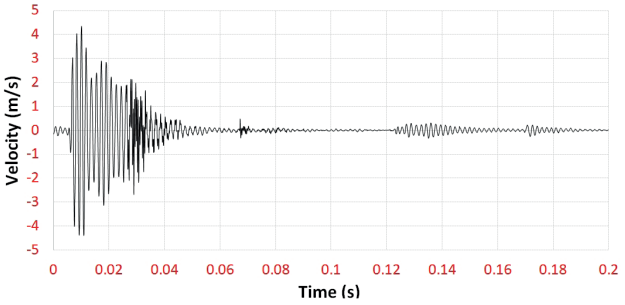

Fig. 6 Seismogram from an example source point and used during the numerical modelling of the dynamic behavior of the rock mass

Focusing on the aspects of the dynamic investigations, no residual values were used to set the parameters, only the elastic settings were activated.

Primary Raylaigh damping values were adjusted based on multiple test runs [24, 25]. The damped frequency range was 0.05–540 Hz and the damping ratio range was 5–20%.

In the case of the dynamic studies, the prepared models were dynamically loaded from one source point in each case and then at the time queries given in the model space it was possible to retrieve all the information (e.g., dynamic displacement, velocity, acceleration). From the many variations, were primarily interesting in X direction accelerograms between different sources and time queries, in which the first arrivals of the P-wave were examined, and the maximum amplitudes were compared to the values measured with the in-situ probe. It was not possible to examine the spectrums quantitatively since the strength and angle of incidence of the hand hammer blows could not be standardized.

6.2 Modelling results

Since in several cases an increase in the P-wave velocity was observed due to the defined fractures (with rough, calcite filling) and a significant decrease in the case of the fracture defined as a clayey zone, which did not coincide with the V_p data obtained during the measurements (Fig. 7).

Due to the stress redistribution effect as well as the acceleration along the fractures, were obtained completely different velocities and amplitudes during the time query readings than during the measurement. Thus, also were created models from which have been erased the fracture systems.

Finally, if in the constructed repository chambers area, the currently accepted stress field was used in the models (K_H = 1.427; K_h = 1.204), the computations resulted good correlations if GSI = 90 value was used for the rock mass but also the P-wave velocity values generally were lower than the measured ones.

6.3 Large scale back-analysis modelling

During the numerical modelling study, several variations were tested with one given geometry. The variations included several rock mass quality values (GSI = 95, 85, 75), with several axial load variations, all without the use of an in-situ stress field load. Due to the limited scope of the study, one case is presented below. The rock mass in the presented example can be considered approximately intact rock (GSI = 95), with the following intact rock parameters: UCS_i = 140 MPa, E_i = 64 GPa, ν = 0.24. For the models, the time series shown in Fig. 6 at the source point was added to the models as an extra dynamic load. In the case of the first model presented, no axial load was applied, while in the case of the second model, an axial load of 100 MPa was added.

In the first case, much lower V_p values were measured at the time query point (100 m from the source point) than when the axial load was used (Figs. 8–12).

In the model space with a simplified geometry and defined as an isotropic material, the V_p increase outlined above can be clearly traced, only as a consequence of the load and thus the stress increase.

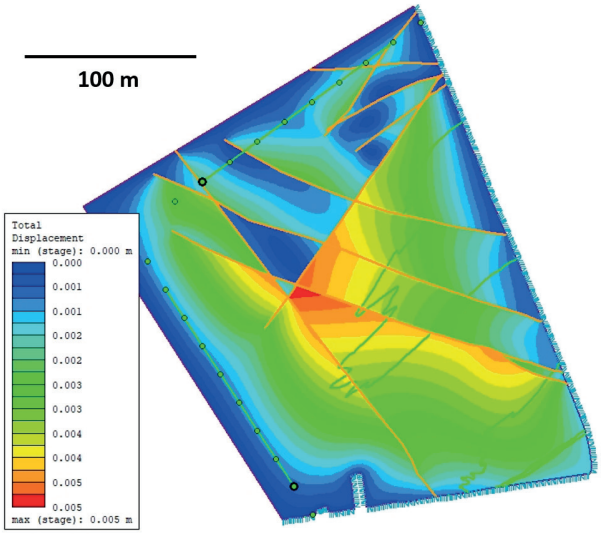

Fig. 7 RS^2 model with clay infilled fractures (orange lines) and lithological boundaries (green lines) – total displacements

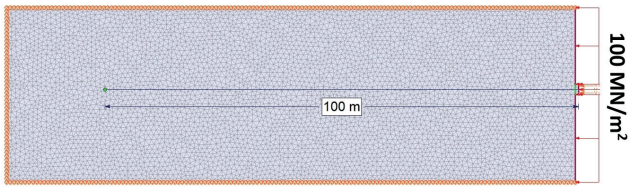

Fig. 8 Large scale numerical model geometry used to study the relationship between P-wave propagation velocity and stress increase in a simplified way

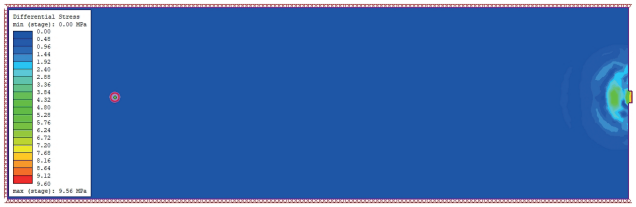

Fig. 9 Large scale numerical model results, with no axial static load, only the activated dynamic load. Differential stress redistribution at stage time 0.01 s (time query from the red circle)

Fig. 10 Large scale numerical model results, with no axial static load, but activated dynamic load. Differential stresses at stage time 0.2 s

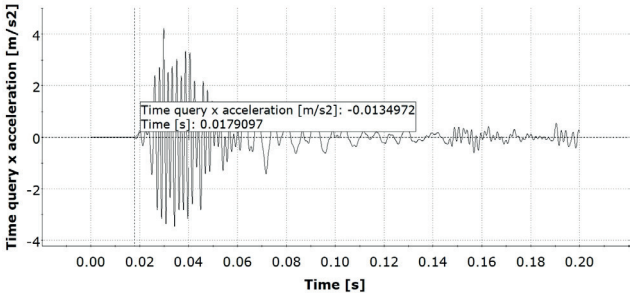

Fig. 11 Accelerogram from the time query from the model with no axial static load (based on the first arrival V_p = 5584 m/s)

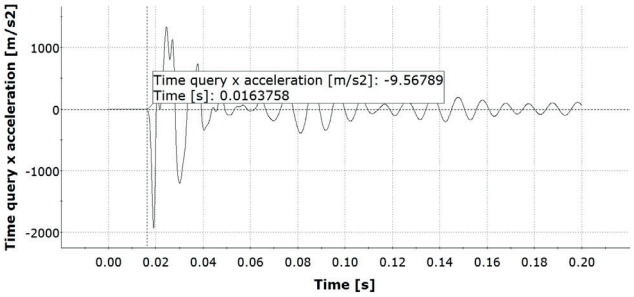

Fig. 12 Accelerogram at the time query from the model with axial static load (based on the first arrival V_p = 6107 m/s)

6.4 Numerical back-analysis modelling of the V_p and stress increase relation of the investigated ground

Aiming to achieve high V_p values, the BeR-19_170_1 raypath was examined.

In this case, the rock physical properties were changed and shifted towards a better rock mass quality, as mentioned, and the rock mass parameters of GSI = 75 and 90 were used.

The results presented below were derived from models with the following major input parameters: GSI = 90, UCS_i = 129, E_i = 64 GPa, ν = 0.25.

The K_H = 1.42 value was tested, originally given in the Geotechnical interpretation report [26], then increased it to K_H = 2 and later reduced it to K_H = 1, the results of two representative models of these experiments are shown in the figures below, where are evidence differences in P-wave velocity as a function of stress increase (Figs. 13–15).

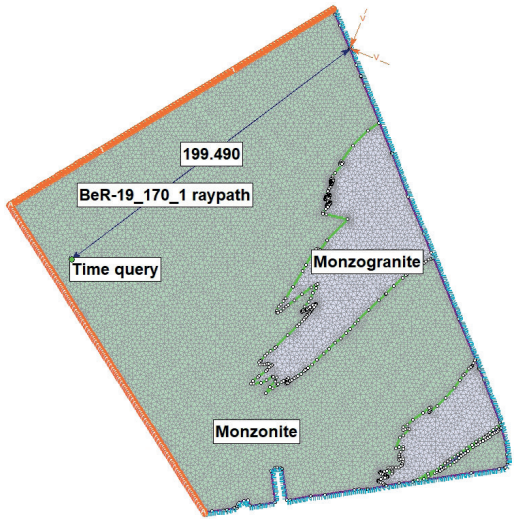

Fig. 13 Model geometry used to study the increase in V_p due to the stress increase and the examined BeR-19_170_1 raypath

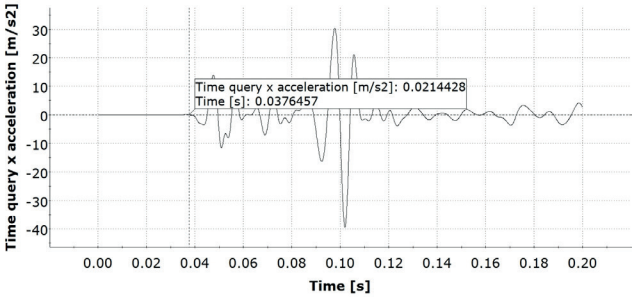

Fig. 14 Accelerogram from the time query of the BeR-19_170_1 raypath for the case when K_H = 1 (based on the first arrival V_p = 5299 m/s)

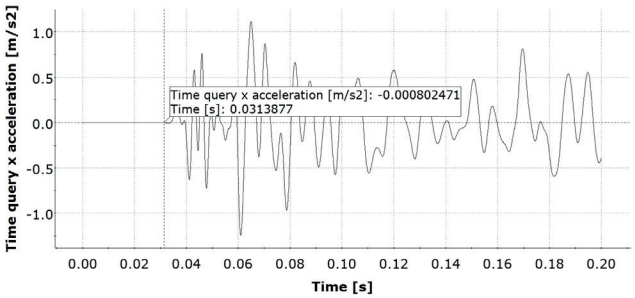

Fig. 15 Accelerogram read at the time query of the BeR-19_170_1 raypath in case of K_H = 2 (based on the first arrival V_p = 6356 m/s)

7 Possible causes and solutions for the observed high P- wave velocities

It was mentioned previously, that did not obtain similarly high V_p values in certain parts of the NRWR according to the assumed boundary conditions. For instance, the current coverage and the stresses measured with recent methods (Doorstopper and CSIRO cell measurements), were more than those measured in the planned extension area where the seismic tomography was carried out. Of course,

it is necessary to mention that some in-situ stress measurements gave higher stress magnitudes for instance, the sleeve fracturing and hydrofracturing results [31].

The previous seismic measurements had similarly high V_p values, including the crosshole measurements in the surface exploration boreholes, and of course during the underground seismic tomographic survey.

The presented differences in P-wave velocity in the rock mass may be due to several reasons: it is possible that the material of the rock mass has higher strength properties than the case laboratory intact samples (this can be ruled out in actual case), or the rock mass strength of the studied rock mass are better than the other excavated areas, which seems to be the case as the modelled results using GSI = 70–90 were better than with lower GSI values. At the same time, it is possible for the boundary conditions to have a stress increase in the rock mass, which may also contribute to an increase in V_p values. As following, the study was dealt with the effect of excess stress on P-wave velocity, which, using the term used in structural geology, may be present as a residual stress in the rock body of the Mórágy block.

7.1 P-wave velocity increase due to stress increase

Numerous sources in the literature deal mainly with the evaluation of the results of rock mechanical laboratory measurements [32, 33] and a much smaller volume of publications on large-scale in-situ stress increase studies can be found [32, 34].

In general, the following observations can be made:

- the increase in V_p is non-linear and the greater appears in the early increasing phase of the stress.
- as the stress continues to increase, the increase in P-wave velocity decreases, in response to which new cracks appear (yielding point) in parallel with the load.
- these observations suggest that high P-wave velocity regions may indicate the presence of high stress concentration zones, while low velocity regions may indicate stress relaxation zones.

One of the large-scale experiments at a mine has similar bedrock to that of the NRWR and the overburden is also similar [32].

The rock masses of the experimental drift system are mostly Precambrian metamorphic and granite rocks (Idaho Springs Formation) [32]. The overburden of the drift system used for the test was 120 m.

A pillar was surrounded with a number of source and receiver points, it was measured in its original state and then a load cell was placed on one side in a slot and a pressure of 20.7 MPa was applied. Seismically measurements on the pillar were repeatedly taken while maintaining this load. Velocities west of the cell increased by about 2.4 km/s, while velocities east of the pressure cell decreased by 2.4 km/s. It was hypothesized by the authors that the harder rock west of the pressure cell (a massive, unfractured biotite microcline pegmatite) retained stress, while the softer rock east of the cell (a massive, biotite schist with numerous fractures) was able to squeeze and absorb stress [32]. However, this scenario was inconsistent with the work of [13], who found that as pressure was exerted on fractures, the fractures closed, and velocities increased.

In summary, geologic structures (faults and some rock types) reflected relatively well in the tomograms. At a small scale (9.2 m), stress changes were seen both in the tomograms and the finite-difference model (modelling was carried out in Flac 3D). Ultrasonic V_p measurements on core specimens correlated well to the P-wave velocity measurements seen in the tomograms.

Based on the mentioned research [32], the use of seismic tomography to identify stress gradients in an underground rock pillar was validated. Furthermore, the use of seismic tomography to detect mine workings could be valuable in locating abandoned mine openings in coal or hard rock.

7.2 Geological events that can result in significant residual stress in rock masses

If just few in-situ stress measurements are available for a given rock mass and small areas can be characterized based on their scale factor (as mentioned earlier for instance with CSIRO cell measurements possible dimension of stress field analyzed is between 10^{-3} to 10^{-2} m^3), then it is definitely worth examining the regional tectonic regime of the target area. If this does not contain information on the basis of which can be assumed additional horizontal stresses, it is still worth researching the path of the characterized rock mass along the vertical axis during the geological eras (creating the subsidence curve).

Voight [35] clearly blamed the mechanism of burial and subsequent erosion for the high horizontal stresses in the shallow depths of the Earth's crust. Among the large number of geological studies, there is a help to this topic, namely the publication that examines the subsidence curve of the Mórágy Block [36] (Fig. 16).

The research area of [36] was subdivided into two structural units that are besides each other, probably due to horizontal movements. The greater part of the research area was composed of the Mórágy Block; that latter is

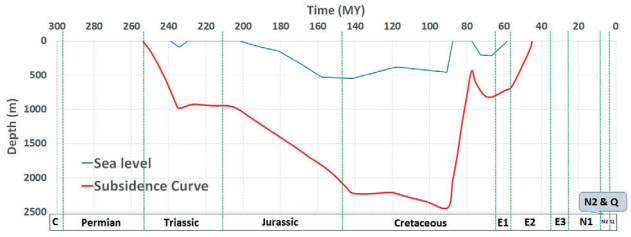

Fig. 16 The subsidence curve of the Mórágy Block. On the geological time axis, the international codes (ICS 2004) are indicated: C = Carboniferous, E1 = Palaeocene, E2 = Eocene, E3 = Oligocene, N1 = Miocene, N2 = Pliocene, Q = Quaternary. Blue line – water depth, Red line – depth to the crystalline basement (after [36])

joined in the NW by a territory called the Zsibrik Block. On the former, the Palaeozoic Mórágy Granite Formation can be found on the surface, predominantly covered by Quaternary or, exceptionally, by thin Upper Miocene – Pliocene sequences. On the NW margin of the block, the Palaeozoic Ófalu Formation is situated. The subsidence histories of the two areas agree in their characteristic features. However, in the area in a more southern position (and more eastern origin, at the same time) the lack of sediments is more significant in the Permian and the Mesozoic, but the greatest difference is derived from the generally higher, range-like nature of the area.

Thus, while the surface of the crystalline formations exceeded even a 4000 m depth in the Late Jurassic – Early Cretaceous in the Zsibrik Area, the surface of the Mórágy Block may have subsided only slightly below 2000 m. Assuming that during the Palaeogene this area uplifted to the same degree as the Zsibrik Area, even 1000 m of the granite may have been eroded and the present-day surface of the crystalline formations may have reached a depth of 3500 m during the subsidence.

In the course of further investigations understanding the residual stress that could remain as a result of a significant burial or subsidence outlined above would be of interest. To address this point empirical equations were used.

There are fewer references in the literature to residual tension due to burial - prominence than to other similar topics in general. One of the classic approaches has been found in our university studies, where Twiss and Moores provide a very useful correlation in their book "Structural geology" [37], but this requires a temperature expansion coefficient in addition to the depth information contained in the subsidence curve. The authors also worked on these correlations, but the verification of the data required for the calculations is still ongoing.

Another empirical correlation was given by Goodman [38], then refined by Bernard Amadei and Stephansson [39], which was used in this study.

In the empirical approach presented, K_0 denotes the initial horizontal-vertical stress ratio at a point at depth z_0 in a rock mass. The rock mass is unloaded by removing the Δz-thick assemblage. Based on the theory of elasticity, it can be shown that the new stress ratio at the depth $z = z_0 - \Delta z$ can be calculated by the following equation:

$$K = K_0 + \left[K_0 - \nu / (1-\nu)\right] \times \Delta z / (z_0 - \Delta z). \quad (1)$$

The maximum subsidence depth of the examined rock mass was assumed to be 3000 m.

In the present calculations, the depth-K diagram developed by Brown and Hoek [40] was used to determine the K_0 value.

Accordingly, the following table (Table 1) the calculate K values from Eq. (1) were obtained.

The empirical calculation results also are justify using higher K values for the numerical modelling for the Future chambers excavation N area, where the seismic tomography was carried out.

8 Conclusions

A seismic tomographic survey, dynamic FEM numerical modelling, empirical calculations of residual stresses, laboratory measurements of compression wave (ultrasonic) velocities in rock cores, in-situ primary stress measurements and site geology were integrated to evaluate the use of seismic tomography for identifying in-situ stress increase. The results indicated that seismic tomography appears to be a useful tool for determining relative stress in underground areas in large scale and space.

The seismic tomographic survey was carried out by using a self-developed high-sensitivity borehole probe which also was used as a specifically mounted receiver on the tunnel walls.

In this research a detailed calibration modelling exercise was carried out, based on the presented site seismic tomography measurements. During the large scale modelling the

Table 1 K values calculated on the basis of the subsidence curve in relation to the Bátaapáti NRWR

K_0	K (calculated)
0.33	0.3
0.5	2
1	7

increasing P-wave velocity in relation by increasing directional loadings on the rock mass were observed. By using a measured wave raypath it was checked the different in-situ stress parametrizations were checked and these give the best approximation to the measured V_p values.

In case of the future extension "Future chambers excavation N" area, very high P-wave velocities were observed during the seismic tomography measurements compared to the excavated "Repository chambers" area. The authors hypothesized that a larger in-situ primary stress field may be characteristic of this area. First, possible residual stress value was calculated by using empirical analytical methods taking into consideration a hypothetical and currently accepted subsidence curve. Subsequently, calculations were performed using numerical back-analysis modelling, which tested the excess stress values to obtain high V_p values similar to the measured V_p values.

The results of two representative models of these experiments showed evidence of differences in P-wave velocity as a function of stress increase.

As final conclusion, a higher K_H value ($K_H = 2$) should be used for future design work and that this value should be verified, once the extension construction is started, with an appropriate number and distribution of in-situ primary stress measurement methods.

Acknowledgement
The authors acknowledge the permission of PURAM to publish this research.

References

[1] Zang, A., Stephansson, O. "Stress Filed of the Earth's Crust", Springer, 2010. ISBN 978-1-4020-8443-0 https://doi.org/10.1007/978-1-4020-8444-7

[2] Mayr, S. I., Burkhardt, H. "Ultrasonic properties of sedimentary rocks: effect of pressure, saturation, frequency and microcracks", Geophysical Journal International, 164(1), pp. 246–258, 2006. https://doi.org/10.1111/j.1365-246X.2005.02826.x

[3] Lozovyi, S., Bauer, A. "From static to dynamic stiffness of shales: frequency and stress dependence", Rock Mechanics and Rock Engineering, 52, pp. 5085–5098, 2019. https://doi.org/10.1007/s00603-019-01934-1

[4] Young, R. P., Maxwell, S. C. "Seismic characterization of a highly stressed rock mass using tomographic imaging and induced seismicity", JGR Solid Earth, 97(B9), pp. 12361–12373, 1992. https://doi.org/10.1029/92jb00678

[5] Ma, X., Westman, E. C., Fahrman, B. P., Thibodeau, D. "Imaging of temporal stress redistribution due to triggered seismicity at a deep nickel mine", Geomechanics for Energy and the Environment, 5, pp. 55–64, 2016. https://doi.org/10.1016/j.gete.2016.01.001

[6] Ma, X., Westman, E., Slaker, B., Thibodeau, D., Counter, D. "The b-value evolution of mining-induced seismicity and mainshock occurrences at hard-rock mines", International Journal of Rock Mechanics and Mining Sciences, 104, pp. 64–70, 2018 https://doi.org/10.1016/J.IJRMMS.2018.02.003

[7] Ma, X., Westman, E., Malek, F., Yao, M. "Stress redistribution monitoring using passive seismic tomography at a Deep Nickel Mine", Rock Mechanics and Rock Engineering, 52, pp. 3909–3919, 2019. https://doi.org/10.1007/s00603-019-01796-7

[8] Westman, E. C., Molka, R. J., Conrad W. J. "Ground control monitoring of retreat room–and–pillar mine in Central Appalachia", International Journal of Mining Science and Technology, 27(1), pp. 65–69, 2017. https://doi.org/10.1016/j.ijmst.2016.11.008

[9] Mercer, R. A., Bawden, W. F. "A statistical approach for the integrated analysis of mine-induced seismicity and numerical stress estimates, a case study—Part I: developing the relations", International Journal of Rock Mechanics and Mining Sciences, 42(1), pp. 47–72, 2005. https://doi.org/10.1016/j.ijrmms.2004.07.006

[10] Friedel, M. J., Jackson, M. J., Scott, D. F., Williams, T. J., Olson, M. S. "3D Tomographic Imaging of Anomalous Conditions in a Deep Silver Mine", Journal of Applied Geophysics, 34, pp. 1–21, 1995. https://doi.org/10.1016/0926-9851(95)00007-O

[11] Friedel, M. J., Scott, D. F., Jackson, M. J., Williams, T. J., Killen, S. M. "3D Seismic Tomographic Imaging of Mechanical Conditions in a Deep U.S. Gold Mine. In Mechanics of Jointed and Faulted Rock-2", In: Proceedings of the International Conference on Mechanics of Jointed and Faulted Rock, Vienna, Austria, 1995, pp. 689–695. ISBN 9789054105411

[12] Friedel, M. J., Scott, D. F., Jackson, M. J., Williams, T. J., Killen, S. M. "3D Seismic Tomographic Imaging of Anomalous Stress Conditions in a Deep US Gold Mine", Journal of Applied Geophysics, 36, pp. 1–17, 1996.

[13] Friedel, M. J., Scott, D. F., Williams, T. J. "Temporal Imaging of Mine-Induced Stress Change Using Seismic Tomography", Engineering Geology, 46, pp. 131–141, 1997. https://doi.org/10.1016/S0013-7952(96)00107-X

[14] Jackson, M. J., Friedel, M. J., Tweeton, D. R., Scott, D. F., Williams, T. "Three-Dimensional Imaging of Underground Mine Structures Using Seismic Tomography", In: Proceedings of the Symposium on the Application of Geophysics to Engineering and Environmental Problems, Orlando, FL, USA, 1995, pp. 221–230. https://doi.org/10.4133/1.2922140

[15] Scott, D. F., Williams, T. J., Friedel, M. J., Denton, D. K. "Relative Stress Conditions in an Underground Pillar, Homestake Mine, Lead, SD", International Journal of Rock Mechanics and Mining Sciences, 34, pp. 278.e1–278.e11, 1997 https://doi.org/10.1016/S1365-1609(97)00235-9

[16] Scott, D. F., Williams, T. J., Denton, D. K. "Use of Seismic Tomography to Identify Geologic Hazards in Underground Mines", The Professional Geologist, 35(7), pp. 3–5, 1998.

[17] Balla, Z. A. "Final report of underground geological research", PURAM report, MÁFI, Budapest, Hungary, Rep. RHK–K–082/08, 2008. (in Hungarian)

[18] Maros, G., Borsody, J., Füri, J., Koroknai, B., Palotás, K., Rálischné, F. E. "Structural geological evaluation of the NE part of the Mórágy block for fracture structures", PURAM report, MÁFI Irattár, Budapest, Hungary, 2011. (in Hungarian)

[19] Szebényi, G., Török, P., András, E., Szamos, I., Mező, Gy., Korpai F., Kovács, L. "Geological summary report. Establishment of the NRWR 2008-2012", PURAM report, Mecsekérc Ltd., Pécs, Hungary, Rep. RHK–K–020/12, 2012. (in Hungarian)

[20] Szebényi, G., Hámos, G., András, E., Török, P., Majoros, Gy., Szamos, I., Molnár, P., Benedek, K., Kovács, L. "Summary assessment report for underground installation design and safety report", PURAM report, Mecsekérc Ltd., Pécs, Hungary, 2009. Rep. RHK-K-181/08, 2009. (in Hungarian)

[21] Prónay, Zs., Madarasi, A., Tildy, P. "Summary report on geophysical tomography between tunnels", PURAM report, RHK Kft., Paks, Hungary, Rep. RHK-K-058/10, 2010. (in Hungarian)

[22] Stewart, R. R., Huddleston, P. D., Kan T. K. "Seismic versus sonic velocities: A vertical seismic profiling study", Geophysics, 49(8), pp. 1153–116, 1964. https://doi.org/10.1190/1.1441745

[23] Deák, F., Szűcs, I. "Dynamic investigations of EDZs from Bátaapáti radwaste repository based on passive seismoacoustic measurements", In: Litvinenko, V. (ed.) Geomechanics and Geodynamics of Rock Masses, Taylor & Francis Group, 2018, pp. 491–498. ISBN 9780429462078

[24] Deák, F., Grabarics, J., Lipovics, T., Sándor, Cs. "Earthquake hazard evaluation of National Radioactive Waste Repository (NRWR) underground facilities" PURAM, Pécs, Hungary, Rep. RHK-K-009/19, 2019. (in Hungarian)

[25] Deák, F., Perras, M. A., Török, Á. "Excavation Damage Zone Behaviour Under Dynamic Loading", presented at ISRM International Symposium - EUROCK 2020, Hard Rock Engineering, Trondheim, Norway, June, 14–19, 2020.

[26] Kovács, L., Deák, F., Somodi, G., Mészáros, E., Máté, K., …., Asszonyi, Cs. "Geotechnical Integration Report, Revision and Expansion of the Geotechnical Interpretation Field Report", PURAM, Pécs, Hungary, Rep. RHK-K-032/12, 2012. (in Hungarian)

[27] Hoek, E., Carranza-Torres, C., Corkum, B. "Hoek-Brown failure criterion-2002 Edition", In: Proceedings of NARMS-TAC Conference, Toronto, Canada, 2002, pp. 267–273. ISBN 0772767068

[28] Hoek, E., Brown, E. T. "The Hoek-Brown failure criterion and GSI -2018", Journal of Rock Mechanics and Geotechnical Engineering, 11(3), pp. 445–463, 2019. https://doi.org/10.1016/j.jrmge.2018.08.001

[29] Diederichs, M. S. "The 2003 Canadian Geotechnical Colloquium: Mechanistic interpretation and practical application of damage and spalling prediction criteria for deep tunnelling", Canadian Geotechnical Journal, 44(9), pp. 1082–1116, 2007. https://doi.org/10.1139/T07-033

[30] Perras, M. A., Diederichs, M. S. "Predicting excavation damage zone depths in brittle rocks", Journal of Rock Mechanics and Geotechnical Engineering, 8(1), pp. 60–74, 2016. https://doi.org/10.1016/j.jrmge.2015.11.004

[31] Kis Herczegh, P. "Results of sleeve fracturing and hydrofracturing measurements from Bátaapáti NRWR", KBFI-ALFA Ltd., Budapest, Hungary, 2015. (in Hungarian)

[32] Scott, D. F., Williams, T. J., Tesarik, D. R., Denton, D. K., Knoll, S. J., Jordan, J. "Geophysical Methods to Detect Stress in Underground Mines", National Institute for Occupational Safety and Health, Spokane, WA, USA, Rep. RI 9661, 2004.

[33] Chen, X., Xu, Z. "The ultrasonic P-wave velocity-stress relationship of rocks and its application", Bulletin of Engineering Geology and the Environment, 76, pp. 661–669, 2017. https://doi.org/10.1007/s10064-016-0866-6

[34] Deák, F., Bakai J. "Kiegészítő szeizmikus átvilágítás" (Additional seismic tomography measurements), PURAM, Pécs, Hungary, Rep. RHK-K-062/18, 2018. (in Hungarian)

[35] Voight, B. "Interpretation of in-situ stress measurements", In: Proceedings of the 1st ISRM Congress, Lisbon, Portugal, 1966, pp. 332–348.

[36] Császár, G. "Alpine burial history of the Mórágy Block and its environs", Annual Report of the Geological Institute of Hungary, 2003, pp. 395–406, 2004.

[37] Twiss, R. J., Moores, E. M. "Structural Geology", W. H. Freeman and Company, 2007. ISBN-13: 978-0-7167-4951-6 https://doi.org/10.1007/s00024-009-0541-y

[38] Goodman, R. E. "Introduction to Rock Mechanics", 2nd ed., Wiley, 1989. ISBN 978-0-471-81200-5

[39] Amadei, B., Stephansson, O. "Rock Stress and Its Measurement", Springer, 1997. ISBN 978-0-412-44700-6 https://doi.org/10.1007/978-94-011-5346-1

[40] Brown, E. T., Hoek, E. "Trends in relationships between measured in situ stresses and depth", International Journal of Rock Mechanics and Mining Sciences & Geomechanics Abstracts, 15, pp. 211–215, 1978. https://doi.org/10.1016/0148-9062(78)91227-5